HHS Public Access

Author manuscript

Appl Phys A Mater Sci Process. Author manuscript; available in PMC 2016 November 01.

Published in final edited form as:

Appl Phys A Mater Sci Process. 2015 November ; 121(3): 1015–1030. doi:10.1007/s00339-015-9508-2.

ToF–SIMS imaging of molecular-level alteration mechanisms in *Le Bonheur de vivre* by Henri Matisse

Zachary E. Voras[1,2], **Kristin deGhetaldi**[3,4], **Marcie B. Wiggins**[1,2], **Barbara Buckley**[5], **Brian Baade**[3], **Jennifer L. Mass**[6], and **Thomas P. Beebe Jr.**[1,2]

Zachary E. Voras: voras@udel.edu

[1]Department of Chemistry and Biochemistry, University of Delaware, Newark, DE 19716, USA

[2]UD Surface Analysis Facility, University of Delaware, Newark, DE 19716, USA

[3]Department of Art Conservation, University of Delaware, Newark, DE 19716, USA

[4]Winterthur-University of Delaware Program in Art Conservation, Winterthur, DE, USA

[5]Department of Conservation, The Barnes Foundation, Philadelphia, PA 19130, USA

[6]Scientific Research and Analysis Laboratory, Conservation Department, Winterthur Museum, Winterthur, DE 19735, USA

Abstract

Time-of-flight secondary ion mass spectrometry (ToF–SIMS) has recently been shown to be a valuable tool for cultural heritage studies, especially when used in conjunction with established analytical techniques in the field. The ability of ToF–SIMS to simultaneously image inorganic and organic species within a paint cross section at micrometer-level spatial resolution makes it a uniquely qualified analytical technique to aid in further understanding the processes of pigment and binder alteration, as well as pigment–binder interactions. In this study, ToF–SIMS was used to detect and image both molecular and elemental species related to CdS pigment and binding medium alteration on the painting *Le Bonheur de vivre* (1905–1906, The Barnes Foundation) by Henri Matisse. Three categories of inorganic and organic components were found throughout *Le Bonheur de vivre* and co-localized in cross-sectional samples using high spatial resolution ToF–SIMS analysis: (1) species relating to the preparation and photo-induced oxidation of CdS yellow pigments (2) varying amounts of long-chain fatty acids present in both the paint and primary ground layer and (3) specific amino acid fragments, possibly relating to the painting's complex restoration history. ToF–SIMS's ability to discern both organic and inorganic species via cross-sectional imaging was used to compare samples collected from *Le Bonheur de vivre* to artificially aged reference paints in an effort to gather mechanistic information relating to alteration processes that have been previously explored using μXANES, SR-μXRF, SEM–EDX, and SR-FTIR. The relatively high sensitivity offered by ToF–SIMS imaging coupled to the high spatial resolution allowed for the positive identification of degradation products (such as cadmium oxalate) in specific paint regions that have before been unobserved. The imaging of organic materials has provided an insight into the extent of destruction of the original binding medium, as well as identifying unexpected organic materials in specific paint layers.

Correspondence to: Zachary E. Voras, voras@udel.edu.

1 Introduction

Henri Matisse's *Le Bonheur de vivre* has long been recognized as an archetype of Fauvist technique, as the artist produced several works between 1905 and 1907 that demonstrate a bold use of line and color [1–3]. In the past decade, however, scientific studies have revealed unforeseen problems associated with Matisse's technique, notably the degradation of the synthetic cadmium yellow (CdS) pigment [4–6]. These findings have prompted the art conservation and scientific communities to conduct further research on Matisse's compositions in an effort to identify the various alteration mechanisms that have led to fading and chalking of passages that would have initially appeared a brilliant yellow [7, 8]. Questions relating to the preventative care of Matisse's works, as well as other painters related to the Fauvist movement, can thus begin to be addressed by developing a better understanding of degradation processes related to CdS pigments. During this industrial period of the nineteenth and twentieth century, new synthetic pigments were on the market for these modern artists; however, many of those pigments are now showing signs of degradation. In addition to yellow cadmium sulfide paints, lead chromate yellow and emerald green have been studied by conservators and scientists due to their degradation. Like cadmium sulfide, lead chromate has been analyzed extensively with XANES and μXRF, showing evidence of photo-oxidative degradation [9, 10]. Emerald green, $Cu(C_2H_3O_2)_2{\cdot}3\ Cu(AsO_2)_2$, on the other hand, has not been as extensively analyzed, but work with FTIR and Raman have shown reactions of free fatty acids to form copper soaps [11].

Previously, various scientific expeditions have sought identification of the inorganic components relating to synthesis and alteration of CdS pigment [4–8]. These results are generally complicated because of the various sources of related cadmium compounds. The photo-induced oxidation products of cadmium yellow follow the path:

$$\mathrm{CdS}+2\mathrm{O_2}+\mathrm{H_2O} \rightleftarrows \mathrm{CdSO_4 \cdot H_2O}, \quad (1)$$

where $CdSO_4 \cdot H_2O$ has the relatively high solubility of 76.4 g/100 mL (3.37 M). This leads to the end-products:

$$\mathrm{CdSO_4 \cdot H_2O}+\mathrm{CO_2} \rightleftarrows \mathrm{CdCO_3}+\mathrm{H_2SO_4}, \quad (2)$$

where $CdCO_3$ is insoluble ($K_{sp} = 1.8 \times 10^{-14}$). While chemically distinct from CdS, these photo-oxidation products can be attributed to either residual material from pigment synthesis ($CdSO_4$, wet process; $CdCO_3$, dry process or indirect wet process) or as a paint additive/paint lightener ($CdCO_3$). Additional cadmium compounds have been identified, including $CdCl_2$ (possible residual starting material from the wet process synthesis of $CdSO_4$), CdC_2O_4 (possible paint additive or acid hydrolysis product), and CdS_2O_3 (possible paint extender), increasing the chemical complexity in studies of CdS pigment.

In prior studies, μXANES, SR-μXRF, and SR-μFTIR have identified the Cd^{II} compounds CdS ($K_{sp} = 1 \times 10^{-27}$), $CdSO_4$ (highly soluble), $CdCO_3$ ($K_{sp} = 1.8 \times 10^{-14}$), $CdCl_2$ and CdC_2O_4 ($K_{sp} = 6 \times 10^{-3}$) in cross-sectional samples taken from *Le Bonheur de vivre*. These results indicate that CdS and $CdCl_2$ are residual starting materials, and that $CdSO_4$, $CdCO_3$, and CdC_2O_4 are most likely photo-induced oxidation products. Also, the appearance of CdS_2O_3 may be an additional by-product of photo-induced oxidation [7, 8]. Giacopetti has done theoretical work on the initial effects of air and humidity (as O_2 and H_2O molecules) on the surface of cadmium sulfide in order to understand the beginning formation of hydrated cadmium sulfate and cadmium carbonate [12]. Currently (see this volume) these same species have been mapped for cross-sectional samples taken from *Le Bonheur de vivre* by 2-D X-ray and SR-μFTIR. For the analyses presented herein, the same samples have been analyzed by ToF–SIMS imaging. It will be shown below that analysis by ToF–SIMS imaging produces data of an analogous quality to that observed by synchrotron-based analytical techniques. This is a beneficial finding, since ToF–SIMS imaging does not require allocated beam-time at a synchrotron facility.

To create *Le Bonheur de vivre*, Matisse likely employed paints bound in a drying oil (e.g., linseed oil), paints that were either drained of the medium prior to application, or significantly thinned using a diluent such as turpentine [1–3]. It appears that Matisse may have been experimenting with a range of organic media including distemper (e.g., collagen-based paints) and casein during this period of his career, something that, along with the drained-oil paints and cadmium sulfide alteration, may be related to the flaking that has been observed on *Le Bonheur de vivre*. To date only a handful of studies have been conducted to characterize the organic binding media present in Matisse's paints and grounds. The current hypothesis strongly supports a depletion of the fatty acids comprising the oil-based binding medium of the painting in the uppermost layers of the paint surface [3, 4, 13]. It has also been hypothesized that the depletion of fatty acids should be inversely correlated with the formation of CdC_2O_4. Such a process could be viewed as a hydrolytic breakdown of the fatty acids in the presence of excess H_2SO_4, present either as a leftover reagent of CdS pigment synthesis, or as a byproduct of photo-induced oxidation of CdS [4].

A complicating factor for most research involving the analysis of art objects is the unavoidable presence of restoration materials. Due primarily to the lack of cohesion between the paint layers (chalking, spalling, etc.), *Le Bonheur de vivre* has had an extensive restoration history involving multiple campaigns, the first dating to even before Albert C. Barnes purchased the painting. Since then the canvas has been lined to an additional canvas support with a glue or glue-paste adhesive (e.g., collagen, starches), varnished with tri- and/or di-terpenoid resins (e.g., dammar), and locally consolidated using a wide range of polyvinyl acetate and ethyl vinyl acetate polymers (e.g., PVA adhesives, BEVA 371) to stabilize insecure areas of paint (predominately the cadmium yellows) [from the Barnes Foundation conservation records]. A recent study performed on Matisse's *Le Luxe II* painting series (1907) was also hampered by the presence of restoration materials, making it difficult to distinguish between the collagen used during a 1966 restoration and the protein-based paint that may have been used by Matisse [13].

Time-of-flight secondary ion mass spectrometry (ToF–SIMS) is an ultra-high vacuum technique useful in identifying elemental information, including isotopic information, and molecular and chemical information inherent to a sample surface [14, 15]. The technique uses a focused, rastered beam of primary ions that collide with a sample surface, causing secondary molecular and atomic fragments of positive, negative, and neutral charge, to ablate into the vacuum. These are then directed into the time-of-flight mass analyzer where they are detected. The emitted secondary fragments are indicative of the sample surface's composition and have an escape depth of roughly 2–10 nm, with 95 % of the emitted particles originating from the uppermost two monolayers, making the technique effectively surface-sensitive. When practiced in its so-called dynamic mode, ToF–SIMS can be used to erode the sample on atomic or molecular scales, producing a depth profile of a sample's composition. When practiced in its so-called static mode, as was the case here, <0.1 % of a sample's surface is consumed or damaged, thus making it possible to do true analysis of the molecular fragments located on a sample surface, consisting in the present case of a paint cross section. Because the primary ion beam is focused and pulsed, these analyses can be conducted in a point-by-point manner on the lateral plane of the sample, resulting in ToF–SIMS images, where each pixel contains information about the molecular fragments and/or elemental species present on the sample surface.

The current technology of Tof–SIMS instrumentation allows for the routine analysis of soft materials [16–18]. This is directly related to advancements in primary ion beams (cluster sources) that provide higher data acquisition rates and increased spatial resolution of the rastered beam [19–22]. Specifically, the use of bismuth clusters has drastically improved secondary ion yield while maintaining a high spatial resolution in the sub-micron level when the sample truly contains interfaces with such structural features [23–25]. Using these cluster sources, ToF–SIMS has shown great promise in the analysis of proteins and various biological materials [26–30]. Additionally, the advent of cluster ToF–SIMS analysis has allowed researchers to study the matrix effects and reproducibility as they relate to soft materials [31, 32].

ToF–SIMS has previously been shown as a useful technique in the field of art conservation [33–36]. The technique has been proven for its ability to co-localize the various components of paint, as well as show signs of binder and/or pigment degradation [37–39]. The instrument's ability to simultaneously image inorganic and organic species (atomic and molecular) provide a practical complement to the various techniques commonly used in the art conservation field, such as scanning electron microscopy, Fourier-transform infrared spectroscopy, and gas chromatography-mass spectrometry [33, 40, 41]. Additionally, ToF–SIMS has the added benefit of providing analysis on and then return of extant samples without the need for additional derivatization or analyte extraction. This benefit allows for the sample to remain chemically unaltered and physically intact for further analysis.

A benefit to ToF–SIMS imaging is the ability to assign chemical identity based on exact mass fragment and isotopic distribution instead of chemical shift based on electronic structure or vibrational structure, such is seen in X-ray techniques, FTIR, and Raman spectroscopy. This can minimize spectral interference that leads to ambiguity in assigning chemical identity. While secondary fragments can have similar masses, the high mass

resolution ($m/\Delta m > 6500$ for most molecular fragments; see specific examples below) afforded by the time-of-flight mass analyzer is able to resolve most potential peak overlaps. Whenever an overlap of analyte peaks is not able to be resolved, it is generally possible to select a different but related analyte peak that corresponds to the chemical species of interest, based on fragmentation of the molecular ion. Similarly, it is beneficial to select and image *multiple* mass fragments resulting from the fragmentation of a single compound of interest to ensure the co-localization of the mass fragments is identical, providing higher confidence in the analysis. Examples of this are given below. Lastly, in direct comparison with the XANES technique that has been used to image the same cross-sectional samples from *Bonheur de vivre*, it is important to understand the benefit and limitation to each analysis. XANES, which requires a synchrotron facility, has the benefit of reliable quantitation but lacks high sensitivity, since the XANES technique is limited to a few ppm for detection [42]. ToF–SIMS, a laboratory-based technique, can have higher sensitivity depending on the sample (on the scale of ppb or better), but is limited in its ability to quantitate absolutely, due to the matrix effect [15, 43].

2 Materials

2.1 Cd-containing standards

To help identify pertinent exact mass fragments, isotopic ratios, and to determine the effect of possible primary-ion-beam-induced chemical alteration, standards were purchased and analyzed by ToF–SIMS using the same parameters used for the analysis of cross-sectional samples taken from the *Le Bonheur de vivre* painting. The selected standards were: CdS (99.999 % metals basis, Alfa Aesar); $CdSO_4 \cdot 8\ H_2O$ (99.996 %, Alfa Aesar); CdC_2O_4 (>98 %, MP Biomedicals); $CdCO_3$ (99.998 % metals basis, Alfa Aesar); and $CdCl_2$ (99.99 % trace metals basis, Acros Organics).

2.2 Historically accurate paint reference standards

In order to generate comparable CdS paint reference samples, historically accurate materials were used to reproduce the paint stratigraphy observed on Matisse's *Le Bonheur de vivre*. A canvas substrate was first prepared in a manner commonly used during the artist's lifetime. The medium-weight linen artists' canvas was first stretched and tacked onto a stretcher frame. Application of sizing layers to limit the absorption of oil into the fabric from subsequent layers followed this. Soaking one part by weight of rabbit-skin glue in 15 parts by volume of distilled water for a few hours, and then dissolving the glue in a double boiler created the sizing material. The warm sizing was then applied to the fabric using a hog's hair brush. A second sizing layer was added after the first layer had dried and had been sanded to remove extraneous fibers and protruding slub threads. A specially prepared ground composed of 60/40 w/w lead white and barium sulfate in linseed oil was made to mimic that found on *Le Bonheur de vivre* in previous studies using SEM–EDS and FTIR [7]. The ground was thinned to a creamy consistency with a small addition of triple distilled English turpentine and was applied with a priming knife. A second layer was added after the first had dried. The canvas was then allowed to cure for a week before the reference paints were applied.

The five reference oil paints were made by first combining the appropriate dry pigments on a tempered sheet of clean glass. Cold-pressed linseed oil was then added dropwise, and the mixture was roughly mixed using a metal palette knife to create a barely workable paste. The pigments were then thoroughly dispersed into the oil using a glass muller. The reference paints were mulled for approximately 15 min until they were smooth, glossy and deemed suitable for application. Glass microscopy slides (Fisher Scientific, 12-544-1) were used to make drawdowns of the dispersed paint samples on the primed glass substrates. The paints were allowed to dry before analysis. The following linseed oil reference paints were created for the study: cadmium sulfide (1.2 g) which was prepared in-house by a precipitation reaction at 50 °C in deionized water using $CdSO_4 \cdot 8H_2O$ (0.02 g/mL) and $Na_2S \cdot 9H_2O$ (0.015 g/mL) solutions. The sodium sulfide solution was poured into the cadmium sulfide solution and stirred, while the reaction mixture cooled to room temperature. The pigment particles were filtered and washed with deionized water repeatedly and gently dried. To prevent the formation of CdO on the surface of the particles, and to most closely replicate the known synthesis procedures followed at the turn of the twentieth century, no calcinations were used.

Various mixtures of pigments were created to account for potential pigment–pigment interactions after a period of artificial aging. Lead white ($2PbCO_3 \cdot Pb(OH)_2$), barium sulfate, and zinc white (ZnO) were sourced from Kremer Pigments (New York). Mixtures included 1:2 cadmium sulfide/lead white; 1:2 cadmium sulfide/zinc white; 1:1:1 lead white/zinc white/cadmium sulfide; and 1:2 cadmium sulfide/cadmium carbonate. The resulting cadmium sulfide particles were characterized by XRD and HR-TEM (data not shown here) and were observed to have an average crystallite size of 2.9 nm.

2.3 Sample locations from '*Le Bonheur de vivre*'

Four samples from *Le Bonheur de vivre* were selected for ToF–SIMS imaging: S6, S112-2, S115, and S117. The sampling nomenclature used here preserves that used in all previous publications so that direct comparisons can be made. The locations on the painting are detailed in Fig. 1. These samples were selected based on both their documented visual changes and because of the extensive synchrotron-based analysis performed on similar samples and regions. S6 was taken from yellow paint near the bottom edge of the painting. S112-2 was taken from the upper-left corner of the painting in the brown foliage area. S115 was taken from the yellow fruit/lemon of the tree on the right of the painting. S117 was taken from yellow paint island in the right foreground region, between the flute player and the reclining couple.

3 Experimental details

3.1 Artificial aging

The historically accurate paint reference samples were subjected to short-term aging at the Getty Conservation Institute using the Atlas Ci4000 Weather-Ometer. This was equipped with a Xenon light source (75,000 lux) and carried out using the ASTM Gamblin oil paint parameters (45 % RH, 25 °C, 400 h). Visible-only and UV-only exposures were carried out on two identical sets of samples. Visible light exposure was carried out for 40 million lux hours, intermediate between ISO Blue Wool 5 and 6. Visual comparison with the reference

set of samples at this point revealed no evidence of photo-aging. The samples were deemed to have surfaces that were too inhomogeneous to measure sub-visible delta E color changes.

3.2 Microscopic examination

Reference and historical samples were analyzed under high magnification using a Nikon Eclipse 80i Binocular Microscope (4×, 10×, and 20× objectives), with a Nikon X-cite® 120 mercury lamp for reflected ultraviolet light. Under ultraviolet light, the samples were viewed using a Nikon BV-2A cube (excitation wavelengths between 400 and 470 nm with barrier filter). Digital images were obtained using a Nikon Digital Eclipse DXM 1200f Camera in conjunction with Automatic Camera Tamer control software for PC operating systems.

3.3 Sample preparation for ToF–SIMS analysis

Sample preparation for ToF–SIMS analysis was performed as detailed in Voras et al. (2014). Unlike for some other applications of microtomy, microtomy was used here to expose a fresh, smooth surface of the sample in cross section for subsequent ToF–SIMS analysis. Due to the friable nature of the paint materials in the historical samples, the ToF–SIMS analysis was performed on the freshly exposed remaining sample surface, and not on the removed thin cross sections. All paint cross sections were imbedded in Extec® polyester resin/hardener (mixed at approximately 10 mL/0.5 mL). All samples were first hand-trimmed using a Dremel® rotary tool prior to fixing the sample onto an aluminum specimen pin using cyanoacrylate glue. After the resin had cured for at least 24 h, the sample surface was then prepared by room-temperature microtomy under normal atmospheric conditions. First, the sample was roughly trimmed with a carbon-steel knife (DDK, Inc.) to remove excess resin. A Leica 2035 Jung Biocut (Leica Instruments, GmbH) was used to remove cross sections <1 μm in thickness with a diamond ultramicrotomy knife (DDK, Inc.). Following this, the sample and specimen pin were placed into a sample holder for ToF–SIMS analysis and placed into the ToF–SIMS sample introduction chamber for immediate pump-down.

3.4 ToF–SIMS parameters

ToF–SIMS analysis was performed on a TOF–SIMS IV, upgraded to the capabilities of a TOF–SIMS V (ION-TOF, GmbH) with a bismuth/manganese primary ion source, housed in the Surface Analysis Facility at the University of Delaware. All spectra and images were acquired in the high-current ‘bunched’ mode, utilizing 25-keV Bi_3^+ clusters having a pre-bunched pulse width of 640 ps and a target current of ~0.27 pA. A low-energy (75 eV) electron flood gun was utilized to offset any charge accumulation on the sample surface. All images were collected at a pixel density of 128 × 128 pixels, and primary ion dose density less than the static SIMS limit of 1×10^{12} ions/cm^2. The extraction cone prior to the time-of-flight mass analyzer was pulsed at ±2 kV depending on the desired secondaryion polarity, and detection used 10 kV post-acceleration. All sample analysis was performed at an analysis chamber pressure of 5.0×10^{-9} mbar or lower.

To estimate the achieved spatial resolution, several ion images of microtomed historical samples were analyzed using the 80–20 % linescan criterion, resulting in an average of 7.5 ± 3.0 μm (n = 11). We interpret this to mean that sample-preparation artifacts stemming from microtome-induced smearing were absent or minimal, since similar measurements on a

silver edge using the same beam conditions resulted in a similar average 80–20 % linescan edge width of 5.3 ± 0.2 μm (n = 10). The small discrepancy in average line width and deviation is explained as the difference between an ideal sample (clean silver edge) and that of an un-ideal sample (microtomed sample containing materials of various hardness).

Positive-ion mass-scale calibration was performed with the following ions: H^+, H_2^+, H_3^+, C^+, CH^+, CH_2^+, CH_3^+, $C_2H_3^+$, $C_3H_5^+$, $C_4H_7^+$, $C_5H_5^+$, $C_6H_5^+$, and $C_7H_7^+$. The negative-ion mass scale was calibrated with the following ions: H^-, H_2^-, C^-, CH^-, CH_2^-, CH_3^-, C_2^-, C_2H^-, C_3^-, C_4^-, C_5^-, C_6^-, and C_7^-.

After calibration, instrumental performance metrics were calculated. For negative-mode spectra, 150 peaks were selected from the 10 cross-sectional samples and used for the calculation of some performance metrics. Mass accuracy was calculated to be 4.7 ± 3.9 (n = 150) mAMU, mass precision was calculated to be 103 ± 44 ppm (n = 150), and mass resolving power ($m/\Delta m$) was calculated to be 6000 ± 800 (n = 150; m values ranged from 2526 to 10,622). For positive-mode spectra, 130 peaks were selected from the 10 cross-sectional samples and used for the calculation of some performance metrics. Mass accuracy was calculated to be 2.8 ± 2.2 mAMU (n = 130), mass precision was calculated to be 29 ± 26 ppm (n = 130), and mass resolving power ($m/\Delta m$) was calculated to be 6100 ± 1200 (n = 130; m values ranged from 2105 to 10,208). These calculated performance metrics were consistent with previous performance metrics on similar samples and indicate that ToF–SIMS analysis was able to achieve mass fragment identification based on exact mass assignment, which when used in conjunction with expected isotopic ratios, allowed for unambiguous peak identification.

All data processing was completed on ION-TOF Measurement Explorer, version 6.2. Ion spectra and ion images were normalized to total ion intensity. ImageJ (version 1.48) was used to produce the positive-mode metal-ion overlay images in Fig. 3.

3.5 Gas-chromatography mass spectrometry (GC–MS)

A single sample for aggregate analysis was collected from the bottom edge of the painting (near sample S6) and was first analyzed for fatty acids, waxes, and resins. It was then prepared for amino acid analysis. To reduce the molecular weight and make the components more volatile, one-step treatment of the samples with MethPrep II reagent (Fisher Scientific-Alltech) converted carboxylic acids and esters to their methyl ester derivatives. The sample was placed in a tightly-capped, heavy-walled vial (100–300 μL) and approximately 100 μL (or less for smaller samples) of 1:2 MethPrep II reagent in benzene was added to the sample. The vial was warmed at 60 °C for 1 h on a heating block, removed from heat, and allowed to cool. Analysis was carried out using a Hewlett-Packard 6890 gas chromatograph equipped with a 5973 mass-selective detector (MSD) and a 7683 automatic liquid injector. Prior to injection the inlet temperature was set to 300 °C and the transfer line temperature for the MSD (SCAN mode) was set to 300 °C. A sample volume (splitless) of 1 μL was then injected onto a 30-m × 250-μm × 0.25-μm film thickness HP-5MS column (5 % phenyl methyl siloxane at a flow rate of 2.3 mL/min). The oven temperature was held at 55 °C for 2 min, then programmed to increase at 10 °C/min to 325 °C where it was held for 10.5 min for

a total acquisition time of 40 min. Methanol was used as the rinse solvent in the syringe preparation.

For subsequent protein analysis, the sample was dried down and then heated for 24 h at 105 °C in 5.5-M HCl in a tightly-capped, heavy-walled vial (100–300 μL). The sample was again evaporated to dryness with a gentle stream of pure N_2. Approximately 100 μL of MTBSTFA +1 %TBDMCS silylating reagent (Pierce Chemical Co.) was added to the sample, and the vial was capped and heated at 60 °C for 1 h prior to injection. Analysis was carried out using the RTLMPREP method on the GC–MS. Samples were analyzed using the Hewlett-Packard 6890 gas chromatogram equipped with 5973 mass-selective detector and 7683 automatic liquid injector. Prior to injection the inlet temperature was set to 300 °C, and the transfer line temperature for the MSD (SCAN mode) was set to 300 °C. A sample volume (splitless) of 1 μL was injected onto a 30-m × 250-μm × 0.25-μm film thickness HP-5MS column (5 % phenyl methyl siloxane at a flow rate of 1.5 mL/min). The oven temperature was held at 50 °C for 2 min, then programmed to increase at 10 °C/min to 325 °C where it was held for 10.5 min for a total acquisition time of 40 min. Hexane was used as the rinse solvent in the syringe preparation.

4 Results

Because of the complex, multi-component, and uncontrolled status of the historical samples, an absolute quantitative analysis by ToF–SIMS was not attempted in this study, nor is it typically attempted. Rather, the results presented here were used to infer trends in the data which relied on the spatial positioning and relative intensities (contrast) of the ion emission distributions of the imaged mass fragments, allowing us to form conclusions concerning CdS and binding medium alteration. It is imperative to identify mass fragments based on exact mass and isotopic ratio to ensure a positive identification. Figure 2 is a reference for the process of identification by exact mass and isotopic profile. The top spectrum is of the $CdCl^-$ mass fragment observed in pure standard $CdCl_2$ powder. Notice the distinct isotopic profile expected from the distribution of both Cd and Cl isotopes found in $CdCl^-$. The corresponding peak areas as isotope abundance (%) are given in Table 1. The bottom spectrum of Fig. 2 is of the same mass region as the top spectrum, although the spectrum was obtained from the S115 sample taken from *Bonheur de vivre*. The $CdCl^-$ mass fragment peaks are the small peaks that are left-deviated from nominal mass. The larger right-deviated peaks are due to hydrocarbons in the S115 binding medium and/or in the resin cube which holds sample S115, since the spectrum shown here is from the total area of analysis, which we know to include the parts of the resin as well as parts of the S115 sample. The $CdCl^-$ isotopic abundance (%) for sample S115 is given in Table 1 in comparison with the pure standard $CdCl_2$ powder. The inset shows a greatly expanded mass axis of the same data, in which it is clear that spectral resolution easily allows for separation and quantification of the CdCl species from the hydrocarbon species. Comparison of the expected isotope ratio (Table 1, column 2) with the observed isotope ratio of the pure $CdCl_2$ standard (Table 1, column 3) shows the expected excellent agreement. On the other hand, comparison of the expected isotope ratio (Table 1, column 2) with the observed isotope ratio for the S115 sample (Table 1, column 4) shows the presence of larger deviations. These deviations in isotopic ratio can

be attributed to overlap of signal from CdS^- and its isotope distribution, as expected from a real-world paint sample known to contain both CdS and $CdCl_2$.

4.1 Reference materials analyzed using ToF–SIMS

In previous studies, the presence of paint alteration products and residual reagents from the synthesis of CdS pigment have been identified by synchrotron-based analyses [7, 8, see this volume]. To confirm that these materials are indeed leftover synthesis reagents, it is necessary to first analyze the Cd-containing references in pure powder form before analyzing new and aged samples in cross-sectional form (spectra and images of the powders are not shown). From the ToF–SIMS analysis of the pure CdS powder, mass fragments were mainly comprised of CdS^- (145.875 *m*/*z*) and $CdSO_4^-$ (209.855 *m*/*z*). The appearance of the $CdSO_4^-$ in the corresponding ToF–SIMS images of the powder film of the standard co-localizes identically to that of the CdS^-, so it is important to distinguish unique fragments by spectral features (exact mass, isotopic profile) and image features (co-localization of mass fragments) to determine identity. Unique mass fragments for the standard $CdCl_2$ were $CdCl^-$ (148.872 *m*/*z*), $CdCl_2^-$ (183.841 *m*/*z*) and $CdCl_3^-$ (218.810 *m*/*z*). No fragments due to additional cadmium compounds focused on in this study were identified in the $CdCl_2$ standard material (such as CdS, $CdSO_4$, and $CdCO_3$). Due to the possibility of overlap of $CdCl_2^-$ with chromate pigment $Cr_2O_5^-$ (183.856 m/z, a difference of 0.015 m/z) signal, ToF–SIMS images shown will be that of the mass fragment $CdCl^-$.

ToF–SIMS analysis of the standards $CdCO_3$ and $CdSO_4$ powder identified several unique mass fragments; however, some key beam-induced alteration was noted. The $CdCO_3$ analysis produced the unique mass fragment $CdCO_3^-$ (173.888 *m*/*z*). In addition, the mass fragments for $CdCO_2^-$ (157.893 *m*/*z*) and $CdCO^-$ (141.899 *m*/*z*) were observed. $CdSO_4$ produced unique fragments for $CdSO_2^-$ (177.865 *m*/*z*), $CdSO_4^-$ (209.855 *m*/*z*) and $CdSO^-$ (161.870 *m*/*z*). However, critically, the analysis of the $CdSO_4$ standard also generated mass fragments for CdS^- (145.875 *m*/*z*) and $CdSO_4O^-$ (225.850 *m*/*z*). This mass is very similar to that of $CdS_2O_3^-$ (225.832 *m*/*z*, a difference of 0.018 *m*/*z*) that could cause a possible misidentification. When these fragments were imaged on the standard $CdSO_4$ powder, all the fragments were found to identically co-localize confirming that they were a result of beam-induced breakdown or rearrangement of the $CdSO_4$ analyte, indicating that the identification of CdS_2O_3 and CdS can be confirmed providing the ToF–SIMS images are not identical to the mass fragment image generated by CdSO4.

To identify unique mass fragments associated with CdC_2O_4, the powdered sample produced signals for $CdC_2O_4^-$ (201.883 *m*/*z*) and CdC_2^- (137.903 *m*/*z*). Due to their chemical similarity, both the $CdCO_3$ and CdC_2O_4 standards produced the mass fragments $CdCO_2^-$ (157.893 *m*/*z*) and $CdCO^-$ (141.899 *m*/*z*), so these mass fragments were not used for identification.

Additional reference paint samples (described above) were prepared to mimic the stratigraphy encountered in cross-sectional samples taken from *Le Bonheur de vivre*, of which only the “pure” cadmium sulfide reference sample is shown herein as a comparison of freshly prepared, unaltered cadmium sulfide pigment. The ToF–SIMS images relating to

positive ion species found in samples S6, S112-2, S115, and S117 are also shown in Figure B for comparison. All samples in this study were analyzed by SEM–EDX to confirm when cadmium yellow (and/or other yellow pigments such as chromium) were present (not shown). Sample S115 included in this study has been previously analyzed with SEM–EDS SR-μXRF, μXANES, and SR-FTIR imaging to begin to probe its alteration history, and sample S117 has been analyzed by SEM–EDS and SR-FTIR imaging [7, 8, see this volume].

4.2 Degradation products associated with CdS reagents and photo-oxidation

The cross-sectional CdS reference sample revealed the presence of a number of sulfates present in the paint layer as well as the ground due to the presence of barium sulfate used in the ground formulation (not shown). In this case it is not clear whether the strong signal for $CdSO_4^-$ in the paint is attributed to the residual cadmium sulfate starting reagent from the pigment synthesis or associated with the photo-oxidation of the CdS due to artificial aging. A low signal for $CdCl^-$ was also detected in the reference sample and, as chlorides were not used as reagents for the CdS synthesis, it is assumed that this trace amount of atmospheric-based chlorine may have become incorporated into the paint during preparation of the reference sample. Of greater interest is the lack of $CdCO_3$ (as represented by the mass fragment $CdCO_3^-$), an insoluble product that has previously been associated with degradation mechanisms involving CdS [5–8]. From this observation we deduce that the protocol and duration used to artificially age the paints may not have been severe enough to drive some of the reactions associated with CdS degradation or that other factors may be involved with these mechanisms (e.g., high humidity/heat, the presence of large quantities of atmospheric chlorides, etc.)

Figure 3 shows the mass fragments associated with residual starting materials and photo-induced oxidation products signal for samples S6, S112-2, S115, and S117 (sampling locations shown in Fig. 1) as well as the photo-aged CdS reference sample. The CdS^- signal has been included as a point of reference of remaining unaltered CdS pigment. Samples S6, S112-2, S115, and S117 all show a fairly uniform distribution of $CdCl^-$ throughout the same CdS^- area, indicating a fairly uniform dispersion of residual $CdCl_2$ contained in the paint layers. This indicates that $CdCl_2$ is an expected impurity in the CdS pigment found throughout *Le Bonheur de vivre*, as it is located in both intact and altered paint layers (samples S112-2 and S115). It should be noted while $CdCl_2$ mimics CdS behavior, that the co-localization is not identical, and certain “hotspots” of either material can be observed. This may be attributed to areas where the CdS and the $CdCl_2$ remain unaltered or may be due to the inhomogeneous nature of the original pigment source. A low signal for $CdCl^-$ was also detected in the CdS reference sample and, as chlorides were not used as starting reagents for the prepared CdS, it is assumed that this trace amount of chlorine may have become incorporated into the paint during preparation of the reference sample.

Another important component of CdS alteration is the formation of $CdSO_4 \cdot nH_2O$, $CdCO_3$, and CdS_2O_3. These materials may cause fading (as they are all white powders) and eventual instability of the paint layer if present, and are products of photo-induced oxidation of CdS as noted in the literature [5–8]. Figure 3 shows the $CdSO_4^-$ and $CdCO_3^-$ signals for samples S6, S112-2, S115, S117, in addition to the photo-aged CdS reference sample. As noted, the

third row consists of images of the mass fragment $CdSO_4O^-$ that are directly identical to that of $CdSO_4^-$, indicating that CdS_2O_3 is not present except for sample S115. Image (L) shows discrete particle formation along the paint layer interfaces and the upper "alteration crust" that is significantly different than the image of mass fragment $CdSO_4^-$. Of particular interest is the images related to $CdCO_3$ formation (middle row) as $CdCO_3$ is not hypothesized as a reagent in the CdS synthesis process for the paints used by Matisse to create *Le Bonheur de vivre*, and its present would indicate photo-induced oxidation CdS pigment alteration [7, 8, see this volume].

Although the reference samples were artificially aged as described above, it is possible that a longer exposure time is necessary to observe this particular species as earlier studies have found $CdCO_3$ to be closely linked to CdS photo-oxidation reactions [7, 8]. This further supports the hypothesis that the $CdSO_4$ signal associated with the cross-sectional reference sample (shown in Fig. 3) is likely due to the large amount of residual soluble sulfides that were used to create the pigment.

In comparing the images in Fig. 3, the $CdSO_4^-$ and CdS^- signals were not found to co-localize, indicating that they are unique fragments pertaining to the identification of photo-induced oxidation products and/or as residual starting material and are not visible due to beam-induced alteration. Sample S6 has a uniform distribution of both $CdSO_4^-$ and $CdCO_3^-$ signal throughout the paint layer. The paint is fairly thin in this region and lacking a protective surface coating, factors that would influence the production of alteration products that might extend throughout the entire thickness of the paint layer. In the upper left region of the paint layer in sample S112-2, the CdS^-, $CdSO_4^-$, and $CdCO_3^-$ signals appear to be somewhat uniform, with slight aggregation toward the surface. The lower right region of paint in sample S112-2 showed a more uniform distribution of $CdSO_4^-$ and $CdCO_3^-$. In the alteration crust of Sample S115 (which fragmented during the casting process), the photo-induced oxidation product $CdS_2O_3^-$ is considered a unique mass fragment as the ToF–SIMS image does not co-localize with $CdSO_4^-$, and has a discrete particle-like appearance. This discrete behavior of $CdS_2O_3^-$ continues into the alteration zone where it stops at the interface between the altered and unaltered regions. $CdSO_4^-$ is nearly uniform throughout the alteration crust and the upper paint layers with signal intensity decreasing into the lower paint layer. $CdCO_3^-$ behaves similarly to $CdSO_4^-$ in its uniformity and location. The location of CdS^- is nearly the opposite of the photo-induced oxidation products in sample S115 suggesting that in some areas the CdS pigment has become altered through oxidation processes. The CdS^- has the strongest signal toward the lower portion of the sample, where the paint layer has been more protected from light damage. Lastly, sample S117 is analogous in the appearance photo-induced oxidation products as the CdS^- present in the thin, upper layer appears to have been completely replaced by $CdSO_4^-$ and $CdCO_3^-$, a definitive marker for the formation of an alteration crust, with the thick, lower paint layers showing minimized photo-induced oxidation product signal.

4.3 Hydrolytic breakdown of long-chain fatty acids

A key feature of ToF–SIMS analysis of paint cross sections is the ability to simultaneously image both inorganic and organic species within a sample. Using this ability it was possible to observe mass fragments related to hydrolytic breakdown of the long-chain fatty acids comprising the binding medium component and also their interaction with CdS pigment. As shown in previous studies, long-chain fatty acids (such as palmitic and stearic) have been imaged in negative-mode in paintings ranging from the fourteenth to the twentieth centuries and are used here to estimate binding medium degradation due to pigment oxidation forcing acidification of the binding medium leading to hydrolytic breakdown of the long-chain fatty acid components of the binding medium [38, 44]. In addition, the formation of oxalates was observed in several of the paint samples, a product that is likely due to pigment–binder interactions resulting from photo-oxidation and/or reactions exacerbated by the application of unoriginal organic materials during previous restoration campaigns.

Figure 4 details the relevant mass fragments for long-chain fatty acids and CdC_2O_4 as observed in the cross-sectional samples collected from *Le Bonheur de vivre* as well as the CdS reference sample. The mass fragment $\mathrm{CdC_2O_4^-}$ was chosen to represent CdC_2O_4 formation with palmitic and stearic acid mass fragments shown to represent binding medium degradation. The CdS reference sample showed expected strong signals for palmitic and stearic acids throughout the paint and ground layers, but no signal for $\mathrm{CdC_2O_4^-}$ due to the freshly prepared and minimal aging of the reference sample. Surprisingly, nearly all of the samples collected from the painting show a significant depletion of fatty acid signals in the uppermost paint layers as previously hypothesized by Leone et al. [4]. Sample S6 shows significant loss of long-chain fatty acids as well as a uniform distribution of $\mathrm{CdC_2O_4^-}$ throughout the paint layer. Although S6 suffered from fragmentation during sample preparation, small areas containing traces of the white ground show relatively strong signals for long-chain fatty acids. A similar trend was observed in Sample S112-2, with the lead-containing ground displaying a strong signal for palmitic and stearic acids. The paint layer in S112-2 is not present as a continuous layer. One section of the paint layer appears to generate strong signals for long-chain fatty acids, suggesting that this particular section of the paint layer may have been protected from light or stabilized during a previous restoration using a consolidant. Conversely, the left (or top) section of the paint layer (an area that was likely exposed to incident light) shows a complete loss of long-chain fatty acid signal, while the $\mathrm{CdC_2O_4^-}$ signal is observed with relative uniformity in all regions containing the CdS pigment.

Samples S115 and S117 do not contain the white ground but do possess examples of an alteration crust that can form atop CdS containing paints. The majority of $\mathrm{CdC_2O_4^-}$ signal in S115 can be found in the alteration crust and the upper paint layer with a portion of higher intensity signal in the interface between the upper and lower paint layers. In addition, the alteration crust and upper paint layers are nearly void of long-chain fatty acid signal, with the lower paint layer containing the strongest signal intensity. While sample S117 also shows low-intensity signal for $\mathrm{CdC_2O_4^-}$ in the upper paint layer, a mass fragment of an isotope of $\mathrm{Cr_2O_6^-}$ overlaps with the signal, giving the false impression that there is larger

build up of oxalates in the lower layer (the lower paint layer in this case does contain chromium yellow). As with S115, the fatty-acid component of sample S117 shows a fairly strong, uniform signal throughout the lower paint layer with a decreased intensity signal in the upper paint layer.

Long-chain fatty acids have been previously identified using ToF–SIMS analysis in easel paintings containing drying oil and egg tempera (egg yolk) that date to the fifteenth-century thus it is surprising to encounter such a low signal for palmitic and stearic acids in a painting dating to 1905/6 [38, 44]. Analysis using gas chromatography–mass spectrometry confirmed the presence of palmitic, stearic, and azelaic acids, the latter confirming the presence of a partially un-oxidized drying oil (see Fig. 6). The sample collected for GC–MS analysis, however, was collected from the bottom edge of the painting, and it is likely that these species represent the oil-containing ground that is exposed along the tacking margin (Fig. 7).

4.4 Detection of amino acid components

Analysis using ToF–SIMS allowed for the co-localization of amino acid fragments in several cross sections collected from the painting, providing some insight into the complicated stratigraphy and restoration history of *Le Bonheur de vivre*, an artwork that was created during a crucial yet experimental period of Matisse's career. Various ToF–SIMS studies have identified unique mass fragments associated with the individual amino acids that are found in large proteins [26, 27, 45]. Additionally, GC–MS studies of aged binding media have identified certain amino acids that are expected to be stable during the expected humidity and temperature fluctuations resulting from storage and display of works of art [46, 47]. Building on this foundation, recent studies have demonstrated the ability of Tof–SIMS to distinguish between egg and animal glue proteins found in paint cross sections [37, 38]. From these studies, it is possible to use the amino acid hydroxyproline to distinguish collagen proteins from egg yolk proteins by univariate methods as the amino acid hydroxyproline is only found in collagen protein and is identified by the unique mass fragment $C_4H_8NO^+$. Images in Fig. 5 show mass fragments for amino acids that were found in the samples collected from *Le Bonheur de vivre.* Shown are mass fragments for glycine (CH_4N^+, 30.034 *m*/*z*) and hydroxyproline ($C_4H_8NO^+$, 86.061 *m*/*z*), while additional amino acid mass fragments (alanine, proline, valine, and isoleucine/leucine) were imaged but not shown to confirm the presence of proteinaceous material. These amino acid fragments were used to identify animal glue in samples collected near or along the outer edges of *Le Bonheur de vivre*, as the hydroxyproline fragment was detected in both S6 and S112-2. GC–MS of a sample collected along the edge of the painting (near S6) also confirmed the presence animal glue protein (Fig. 6). In both cases, it is difficult to confirm the original source of the glue, as this material could have possibly been used during the an early restoration lining or may even be residue associated with strips of linen tape that were later adhered to the outer edges (likely containing a glue or gum-glue adhesive). Gel electrophoresis and liquid chromatography mass spectrometry (LC–MS) techniques were used to identify animal glue (bovine source) on Matisse's *Le Luxe II* painted in 1907 [13]; however, the painting was both lined and consolidated with gelatin (source unidentified) making it difficult to confirm whether Matisse was in fact experimenting with a "distemper" medium.

Samples collected from the center of the painting (S115, S117) also showed inconsistent results relating to signals corresponding with amino acid fragments. Sample S117 showed extremely low signals for amino acids, while S115 showed moderate signals for Glycine, Alanine, and Proline, but no signal for hydroxyproline. Unexpectedly, the protein signals co-localize with the upper paint layer(s) in S115 further indicating that the protein source is most likely not from a glue-based lining adhesive applied to the back of the canvas (especially as no amino acids were detected in the ground layer seen in S112-2). Further analysis is needed to confirm the protein source observed in S115 although it appears that animal glue is unlikely due to the poor signal for hydroxyproline. Although recent studies attribute Matisse's purported use of "distemper" to animal glue, archival sources also suggest the use of casein paint, a protein source that has not been extensively studied using ToF–SIMS. As Matisse appears to have used an oil-containing ground for *Le Bonheur de vivre*, applications of an aqueous medium would likely have given rise to a reticulating pattern, a visual effect caused by surface tension between the aqueous medium and the slick oil ground [44]. This effect is not observed in the paint layers used to create *Le Bonheur de vivre*, although one cannot exclude the possibility that Matisse may have manipulated his paints using additives or other methods to promote better adhesion to his oil-primed canvas. Additional research is necessary to confirm whether the amino acid fragments found in S115 are associated with restoration materials (e.g., glue-based adhesive) or reflect Matisse's exploratory painting technique.

5 Conclusion

ToF–SIMS analysis was performed on multiple samples taken across the Henri Matisse painting *Le Bonheur de vivre* (1905/6). The results shown relating to CdS pigment alteration are consistent with those measured by various synchrotron-based techniques (7, 8, see this volume). While the inorganic species were not quantified by ToF–SIMS, they were spatially imaged with resolution down to 4.5 μm. CdS pigment was identified throughout the four analyzed samples, with the residual $CdCl_2$ co-localized throughout the paint layers. The products $CdSO_4$ and $CdCO_3$ identified the photo-oxidation mechanism of alteration for CdS pigment as a possible source of fading/chalking of the once-bright yellows in *Le Bonheur de vivre*. Additionally, organic analysis by ToF–SIMS confirmed the hydrolytic breakdown of the binding medium, leading to the production of CdC_2O_4 and depletion of long-chain fatty acids as a possible mechanism that leads to the friability of the upper paint layers of *Le Bonheur de vivre*.

Furthermore, previous studies conducted by Leone et al. [4] suggest that high humidity promotes the formation of sulfuric acid in CdS paints, contributing to acid hydrolysis of the oil medium. While the painting may have been exposed to high levels of humidity prior to its arrival at the Barnes Foundation, significant amounts of heat and water were undoubtedly used during the glue/paste lining process early in the paintings history. While the complicated restoration history of the picture may relate to the low yield of fatty acid fragments, this observation may also relate to various techniques employed by the artist. By this point in his career Matisse had become enamored with the dry and colorful surfaces he encountered on wall paintings during his excursions throughout France and Italy [1, 3]. Consequently several paintings created during this period exhibit a dry, matte-like quality, a

characteristic at is also associated with *Le Bonheur de vivre* [1, 13]. While Matisse may have been experimenting with aqueous media to achieve this effect it is also possible that the artist sought alternative methods such as draining the excess oil from his tube paints and/or excessively diluting the colors using a solvent such as turpentine [13]. Either method would have created paint layers containing extremely low concentrations of drying oil, possibly explaining why certain passages of the composition appear under-bound and have occasionally suffered from flaking. A non-CdS containing sample, collected from the green foliage, also showed a complete lack of fatty acids when analyzed using ToF–SIMS (not discussed), further suggesting that this phenomenon may not be solely attributed to interaction with CdS pigments.

As this study was primarily focused on the analysis of chemical alteration due to CdS pigment, further analysis is required to understand the role of pigment–binder interactions to fully assess the chemical alteration present in *Le Bonheur de vivre.* Further analysis is necessary to confirm the exact nature of Matisse's ground(s) present in *Le Bonheur de vivre*, but ToF–SIMS did confirm the use of a lower lead-white/barium sulfate containing ground and revealed that it was bound in a drying oil, a layer that is present across the entire canvas. According to visual examination of the painting, two grounds are present on the composition, with the second being less continuous and applied to local areas of the composition. Moreover the interactions between original paint material and applied conservation treatments must also be investigated to determine if these previous campaigns had (if any) significant contributions to chemical alteration of the paintings by Matisse and his contemporaries.

Acknowledgments

We thank Emre Yassitepe and Dr Ismat Shah for preparation of the historically accurate CdS paint material, Derrick Allen for the fabrication of specimen sample holders, and Chris Peterson for his GC–MS analysis. The authors acknowledge the NSF (94-13498; 97-24307) and the NIH NIGMS COBRE program (P30-GM110758) for partial support of activities in the University of Delaware Surface Analysis Facility.

References

1. Barr, AH. Matisse: his art and his public. Museum of Modern Art; New York: 1951.
2. Spurling, H. The unknown Matisse: a life of Henri Matisse, the early years 1869–1908. Alred A Knopf; New York: 1998.
3. Aagesen, D.; Rabinow, R. Matisse: In search of true painting. Metropolitain Museum of Art; New York: 2012.
4. Leone, B., et al. The Deterioration of Cadmium Sulphide Yellow Artists' Pigments. Triennial meeting (14th); The Hague. 12–16 September 2005; James & James; 2005. preprints
5. Van der Snickt G, et al. Characterization of a degraded cadmium yellow (CdS) pigment in an oil painting by means of synchrotron radiation based X-ray techniques. Anal Chem. 2009; 81(7):2600–2610. [PubMed: 19278249]
6. Van der Snickt G, et al. Combined use of synchrotron radiation based micro-X-ray fluorescence, micro-X-ray diffraction, micro-X-ray absorption near-edge, and micro-fourier transform infrared spectroscopies for revealing an alternative degradation pathway of the pigment cadmium yellow in a painting by Van Gogh. Anal Chem. 2012; 84(23):10221–10228. [PubMed: 22931047]
7. Mass JL, et al. The photodegradation of cadmium yellow paints in Henri Matisse's *Le Bonheur de vivre* (1905–1906). Appl Phys A. 2013; 111(1):59–68.

8. Mass J, et al. SR-FTIR imaging of the altered cadmium sulfide yellow paints in Henri Matisse's *Le Bonheur de vivre* (1905–1906)—examination of visually distinct degradation regions. Analyst. 2013; 138(20):6032–6043. [PubMed: 23957052]
9. Monico L, et al. Full spectral XANES imaging using the Maia detector array as a new tool for the study of the alteration process of chrome yellow pigments in paintings by Vincent van Gogh. J Anal At Spectrom. 2015; 30:613–626.
10. Monico L, et al. Synchrotron-based X-ray spectromicroscopy and electron paramagnetic resonance spectroscopy to investigate the redox properties of lead chromate pigments under the effects of visible light. J Anal At Spectrom. 2015; 30:1500–1510.
11. Keune K, Boon JJ, Boitelle R, Shimadzu Y. Degradation of emerald green in oil paint and its contribution to the rapid change in colour of the *Descente des vaches* (1834–1835) painted by *Théodore Rousseau*. Stud Conserv. 2013; 58:199–210.
12. Giacopetti L, Satta A. Degradation of Cd-yellow paints: ab initio study of the adsorption of oxygen and water on {10.0} CdS surface. J Phys Conf Ser. 2014; 566:012021.
13. Segel, K. Jensen ON *Henri Matisse, Le Luxe II*. In: Larsen, PN., editor. SMK ArtJournal. Copenhagen: 2010–2011. p. 149-155.
14. Benninghoven A. Chemical analysis of inorganic and organic surfaces and thin films by static time-of-flight secondary ion mass spectrometry (TOF–SIMS). Angew Chem Ed Engl. 1994; 33:1023–1043.
15. Vickerman, JC. Surface Analysis: The Principal Techniques. 2nd. Vickerman, JC.; Gilmore, I., editors. Wiley; Chichester: 2009. p. 113-205.
16. Cliff B, et al. Development of instrumentation for routine ToF-SIMS imaging analysis of biological material. Appl Surf Sci. 2003; 203:730–733.
17. Brunelle A, Touboul D, Laprévote O. Biological tissue imaging with time-of-flight secondary ion mass spectrometry and cluster ion sources. J Mass Spectrom. 2005; 40:985–999. [PubMed: 16106340]
18. Passerelli MK, Winograd N. Lipid imaging with time-of-flight secondary ion mass spectrometry (ToF–SIMS). Biochim Biophys Acta. 2011; 1811:976–990. [PubMed: 21664291]
19. Kötter F, Benninghoven A. Secondary ion emission from polymer surfaces under Ar^+, Xe^+ and SF_5^+ ion bombardment. Appl Surf Sci. 1998; 133:47–57.
20. Dubey M, Brison J, Grainger DW, Castner DG. Comparison of Bi(1), Bi(3) and C(60) primary ion sources for ToF-SIMS imaging of patterned protein sample. Surf Interface Anal. 2011; 43:261–264. [PubMed: 21516225]
21. Touboul D, et al. Tissue molecular ion imaging by gold cluster ion bombardment. Anal Chem. 2004; 76:1550–1559. [PubMed: 15018551]
22. Kordys J, Fletcher JS, Lockyer NP, Vickerman JC. Substrate effects on the analysis of biomolecular layers using Au^+, Au_3^+ and C_{60}^+ bombardments. Appl Surf Sci. 2008; 255:890–892.
23. Kersting R, et al. Influence of primary ion bombardment conditions on the emission of molecular secondary ions. Appl Surf Sci. 2004; 231–232:261–264.
24. Touboul D, et al. Improvement of biological time-of-flight secondary ion mass spectrometry imaging with a bismuth cluster ion source. J Am Soc Mass Spectrom. 2005; 16:1608–1618. [PubMed: 16112869]
25. Seah MP, Green FM, Gilmore IS. Cluster primary ion sputtering: secondary ion intensities in static SIMS of organic materials. J Phys Chem. 2010; C 114:5351–5359.
26. Wagner MS, Castner DG. Characterization of adsorbed protein films by time-of-flight secondary ion mass spectrometry with principal components analysis. Langmuir. 2001; 17:4649–4660.
27. Xia N, et al. Time-of-flight secondary ion mass spectrometry analysis of conformational changes in adsorbed protein films. Langmuir. 2002; 18:4090–4097.
28. Henry M, Dupone-Gillain C, Bertrand P. Conformation change of albumin adsorbed on polycarbonate membranes as revealed by ToF–SIMS. Langmuir. 2003; 19:6271–6276.
29. Wagner MS, et al. Quantitative time-of-flight secondary ion mass spectrometry for the characterization of multicomponent adsorbed protein films. Appl Surf Sci. 2003; 203–204:704–709.

30. Richter K, Nygren H, Malmberg P, Hagenhoff B. Localization of fatty acids with selective chain length by imaging time-of-flight secondary ion mass spectrometry. Microsc Res Tech. 2007; 70:640–647. [PubMed: 17393479]
31. Green FM, et al. Static SIMS–VAMAS interlaboratory study for intensity repeatability, mass scale accuracy and relative quantification. Surf Interface Anal. 2010; 42:129–138.
32. Shard AG, et al. The matrix effect in organic secondary ion mass spectrometry. Int J Mass Spectorm. 2015; 377:599–609.
33. Keune K, Boon JJ. Secondary ion mass spectrometry of a paint cross section taken from an early Netherlandish painting by Rogier van der Weyden. Anal Chem. 2004; 76:1374–1385. [PubMed: 14987095]
34. Boon JJ, et al. Imaging analytical studies of lead soaps aggregating in preprimed canvas used by the Hudson river school painter FE Church. Microsc Microanal. 2005; 11:444–445.
35. Adriaens A, Dowsett MG. Applications of SIMS to cultural heritage studies. Appl Surf Sci. 2006; 252:7096–7101.
36. Mazel V, et al. chemical imaging techniques for the analysis of complex mixtures: new application to the characterization of ritual matters on African wooden statuettes. Anal Chim Acta. 2006; 570:34, 40.
37. Atrei A, et al. Chemical characterization of protein based binders in painting samples by means of ToF-SIMS: tests on ancient and model samples. Int J Mass Spectrom. 2014; 369:9–15.
38. Voras ZE, et al. Comparison of oil and egg tempera paint systems using time-of-flight secondary ion mass spectrometry. Stud Conserv. 2014; doi: 10.1179/2047058414Y.0000000154
39. Atrei A, et al. An integrated approach to the study of a reworked painting "*Madonna with child*" attributed to Pietro Lorenzetti. J Cult Herit. 2014; 15:80–84.
40. Richardin P, et al. Identification of different copper green pigments in renaissance paintings by cluster TOF–SIMS imaging analysis. J Am Mass Spectrom. 2011; 22:1729–1736.
41. Sanyova J, et al. Unexpected materials in a rembrandt painting characterized by high spatial resolution cluster TOF–SIMS imaging. Anal Chem. 2011; 83:753–760. [PubMed: 21218778]
42. Heald S. Strategies and limitations for fluorescence detection of XAFS at high flux beamlines. J Synchrotron Radiat. 2015; 22:436–445. [PubMed: 25723945]
43. Salter TL, et al. A comparison of SIMS and DESI and their complementarities. Surf Interface Anal. 2011; 43:294–297.
44. Kerr, A., et al. Deconstructing the stratigraphy of color and design in the artistic works of Henry Ossawa Tanner. In: Bridgland, J., editor. ICOM Committee for Conservation, 17th Triennial Conference Preprints; Melbourne. 15–19 September 2015; Paris: International Council of Museums; p. 8art. 1306
45. Henry M, Bertrand P. Surface composition of insulin and albumin adsorbed on polymer substrates as revealed by multivariate analysis of ToF–SIMS data. Surf Interface Anal. 2009; 41(2):105–113.
46. Schilling MR, Khanjian HP. Gas chromatographic analysis of amino acids as ethyl chloroformate derivatives. Part 2: the effects of pigments and accelerated aging on the identification of proteinaceous binding media. J Am Inst Conserv. 1996; 35:123–144.
47. Schilling, MR.; Khanjian, HP. Gas chromatographic analysis of amino acids as ethyl chloroformate derivatives. Part 3: the identification of proteinaceous binding media by the interpretation of amino acid composition data. ICOM Committee for Conservation, 11th Triennial Meeting; Edinburgh. London: James & James; p. 220-227.Preprints

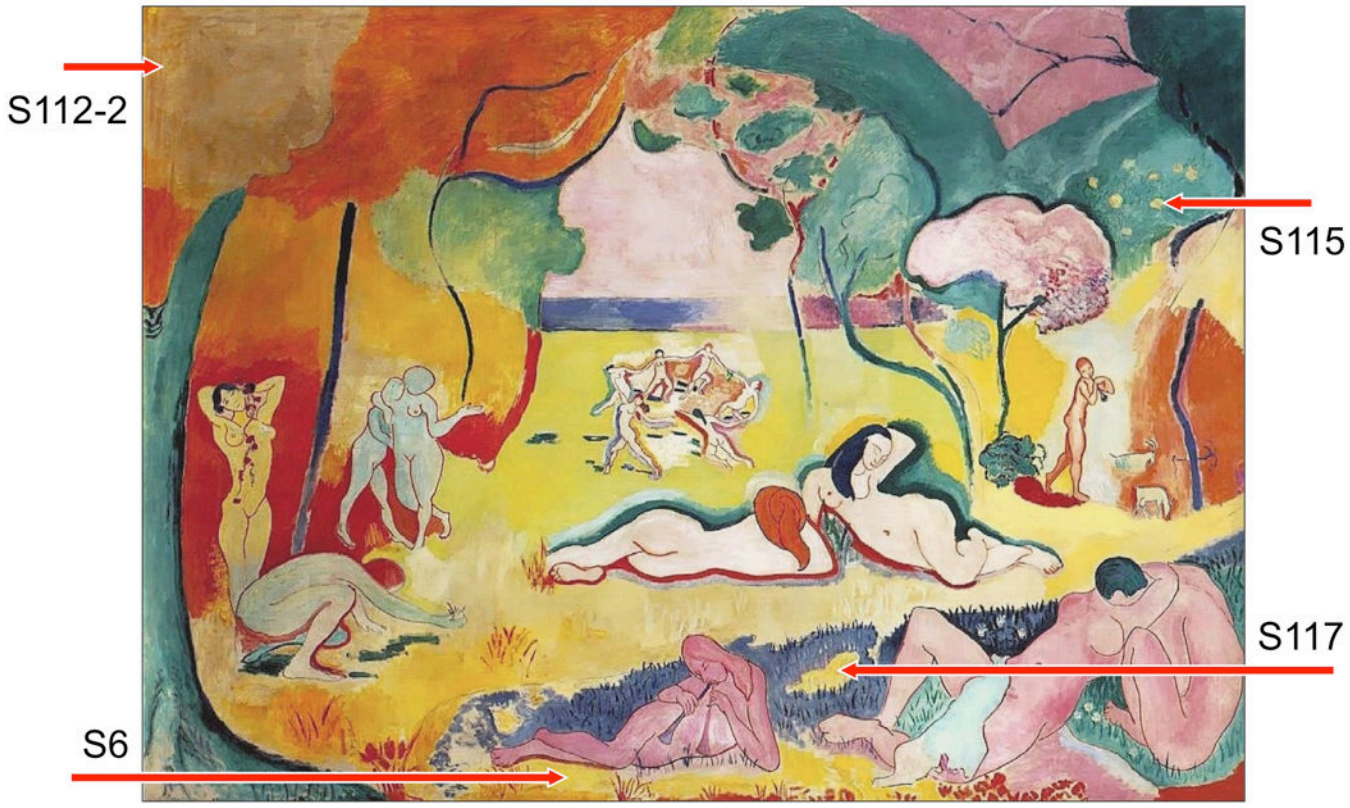

Fig. 1.

Sampling locations on *Le Bonheur de vivre*. Sample S6 and S112-2 were taken on the outer edges of the painting, while S115 and S117 were taken from the inner portion

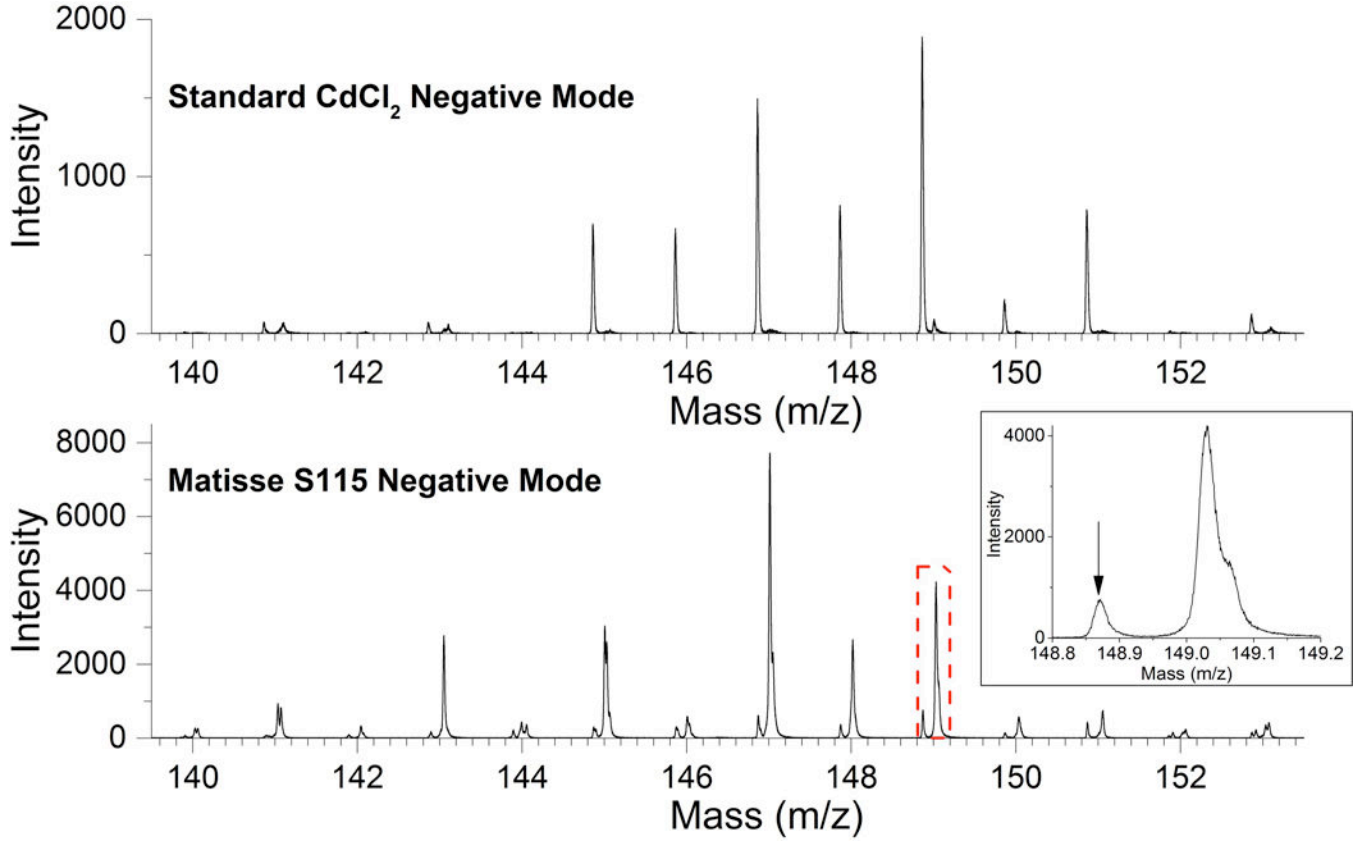

Fig. 2.

Negative-mode ToF–SIMS mass spectra showing isotopic profile of cadmium-containing species. The $CdCl^-$ mass fragment that was used to image $CdCl_2$ impurity in cadmium yellow pigment was selected for representation. The top spectrum resulted from the analysis of the pure reference $CdCl_2$ powder. Note the minimal hydrocarbon peaks that are right-shifted of nominal mass. The bottom spectrum was obtained from the analysis of *Bonheur de vivre* sample S115. In contrast to the pure standard powder, the right-shifted hydrocarbon peaks are major components of the spectrum, whereas the left-shifted inorganic peaks are now minor components in the inset spectrum. The *arrow* in the *inset* points to the $CdCl^-$ mass fragment at *m/z* 148.873. A comparison of expected isotope ratios and calculated isotope ratios for these spectra is given in Table 1

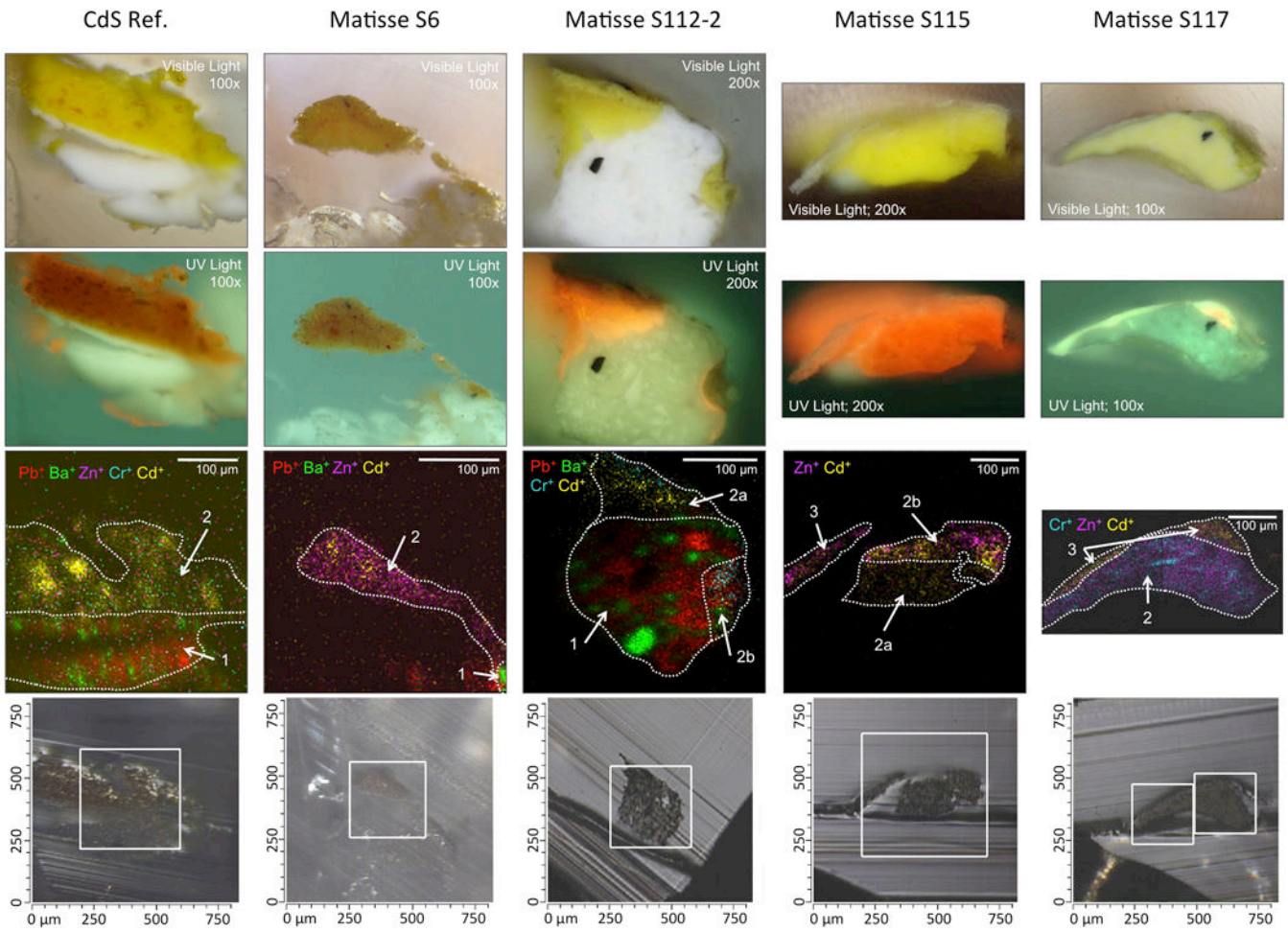

Fig. 3.

Optical images and positive-mode overlay of metal ions in the various samples (from *left to right*: the CdS reference sample, S6, S112-2, S115, S117). The first (*top*) row is the visual image taken after ToF–SIMS analysis. The second row is the same image, but taken with ultraviolet illumination. The third row is an overlay of positive metal ions identified in the samples. The *dotted lines* are drawn to highlight the different layers. For all samples, layer "1" is the ground layer (only present on the CdS reference, S6, and S112-2). Layer "2a" is considered the "lower" paint layer, which is usually protected against significant alteration by "2b" the upper paint layer. Lastly, for samples showing significant amounts of alteration, the "3" layer closest to atmosphere has formed into an "alteration crust". The fourth (*bottom*) row is the optical image from the ToF–SIMS, with the *outlined white box* being the area of analysis. Note that S117 was large enough to consist of two analysis areas within one image without the risk of oversampling effects, with the two images being processed together in ImageJ

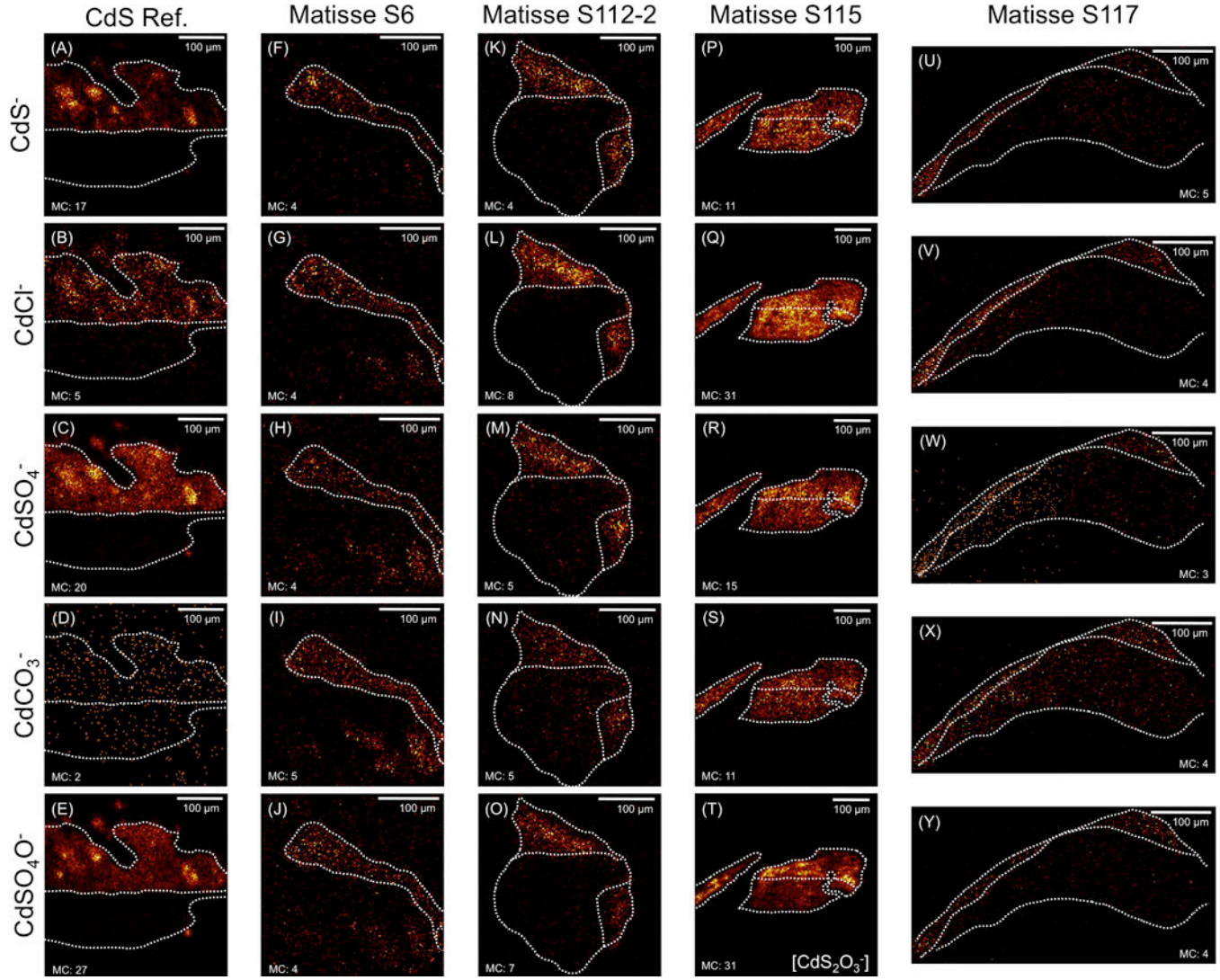

Fig. 4.

ToF–SIMS images of the mass fragments associated with residual starting materials and/or photo-induced oxidation of CdS pigment observed in the various cross-sectional samples taken from *Le Bonheur de vivre*. Dotted outlines correlate to described layers as detailed in Fig. 1. The first (*top*) row of images corresponds to the emission distribution of CdS^- mass fragment (average 145.870 *m*/*z*) that is used to represent unaltered CdS pigment. The *second row of images* corresponds to the emission distribution of $CdCl^-$ mass fragment (average 148.873 *m*/*z*) that is used to represent residual $CdCl_2$ from the CdS synthesis process. The individual samples are sorted into columns as labeled. The *third row of images* corresponds to the emission distribution of $CdSO_4^-$ (average 209.852 *m*/*z*) that is used to represent the soluble $CdSO_4$ oxidation product. The *fourth row of images* corresponds to the emission distribution of $CdCO_3^-$ (average 173.892 *m*/*z*) that is used to represent the insoluble $CdCO_3$ oxidation product. The fifth (*bottom*) row of images corresponds to the emission distribution of $CdSO_4O^-$ (average 225.850 *m*/*z*) that corresponds to either $CdSO_4$ if spatially identical to $CdSO_4^-$ or to $CdS_2O_3^-$ if spatially different. The first column is the CdS reference paint

sample showing (A) CdS^- emission distribution with maximum intensity per pixel (MC) = 17, and the total ion count per image (TIC) = 9.720×10^3; (B) $CdCl^-$ emission distribution, MC = 5, TIC = 3.092×10^3; (C) $CdSO_4^-$ emission distribution, MC = 20, TIC = 2.343×10^4; (D) $CdCO_3^-$ emission distribution, MC = 2, TIC = 5.380×10^2; (E) $CdSO_4O^-$ emission distribution, MC = 27, TIC = 2.331×10^4. The second column is sample S6 showing (F) CdS^- emission distribution, MC = 4, TIC = 8.210×10^2; (G) $CdCl^-$ emission distribution, MC = 4, TIC = 1.252×10^3; (H) $CdSO_4^-$ emission distribution, MC = 4, TIC = 1.546×10^3; (I) $CdCO_3^-$ emission distribution, MC = 5, TIC = 2.289×10^3, (J) $CdSO_4O^-$ emission distribution, MC = 4, TIC = 1.570×10^3. The third column is sample S112-2 showing (K) CdS^- emission distribution, MC = 4, TIC = 1.384×10^3; (L) $CdCl^-$ emission distribution, MC = 8, TIC = 3.515×10^3; (M) $CdSO_4^-$ emission distribution, MC = 5, TIC = 1.928×10^3; (N) $CdCO_3^-$ emission distribution, MC = 5, TIC = 1.154×10^3, (O) $CdSO_4O^-$ emission distribution, MC = 7, TIC = 2.267×10^3. The fourth column is sample S115 showing (P) CdS^- emission distribution, MC = 11, TIC = 7.562×10^3; (Q) $CdCl^-$ emission distribution, MC = 31, TIC = 2.912×10^4; (R) $CdSO_4^-$ emission distribution, MC = 15, TIC = 1.040×10^4; (S) $CdCO_3^-$ emission distribution, MC = 11, TIC = 6.301×10^3; (T) Due to the formation of discrete particles at the layer interfaces and in the alteration crust, $CdS_2O_3^-$ emission distribution, MC = 5, TIC = 1.154×10^3. The fifth column is sample S117 showing (U) CdS^- emission distribution, MC = 5, TIC = 1.195×10^3; (V) $CdCl^-$ emission distribution, MC = 6, TIC = 2.218×10^3; (W) $CdSO_4^-$ emission distribution, MC = 3, TIC = 9.350×10^2; (X) $CdCO_3^-$ emission distribution, MC = 4, TIC = 2.057×10^3, (Y) $CdSO_4O^-$ emission distribution, MC = 4, TIC = 1.043×10^3

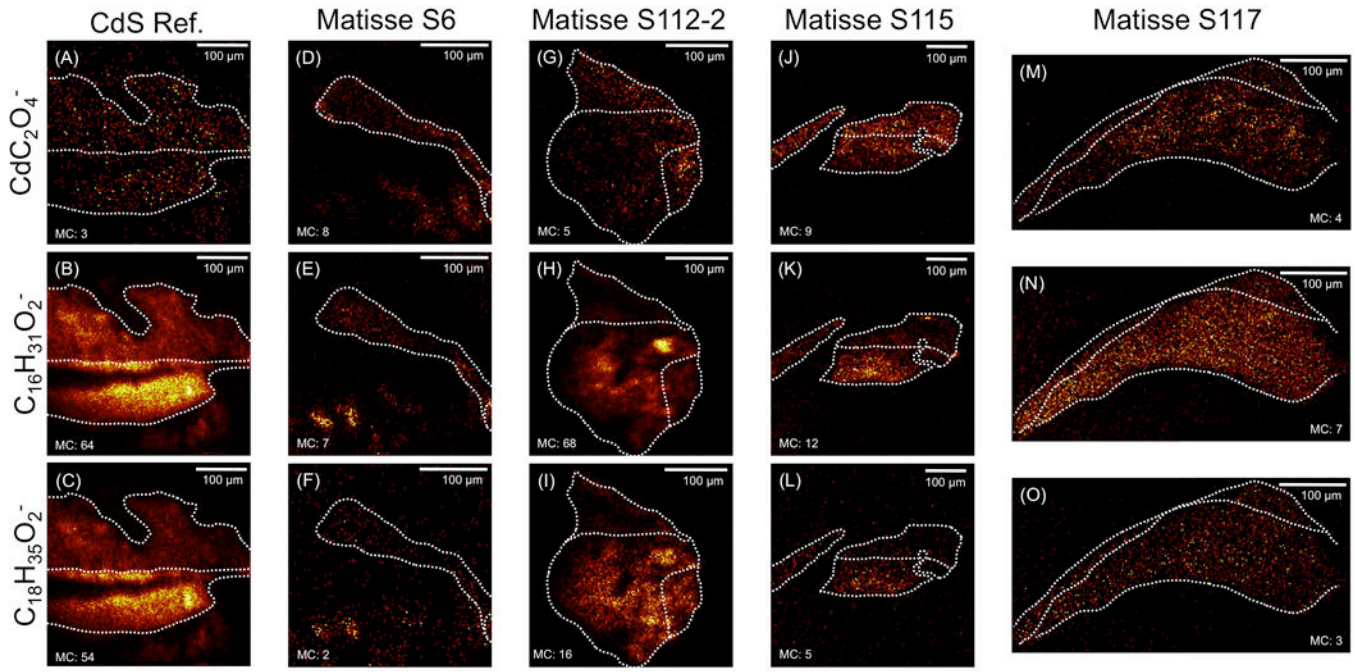

Fig. 5.

ToF–SIMS images of the mass fragments associated with hydrolytic breakdown of long-chain fatty acids in the binding medium of the cross-sectional samples taken from *Le Bonheur de vivre*. *Dotted outlines* correlate to described layers in Fig. 1. The first (*top*) row of images corresponds to the emission distribution of $CdC_2O_4^-$ (average 201.880 *m*/*z*) that is used to represent the CdC_2O_4 hydrolysis product. The second (*middle*) row of images corresponds to the emission distribution of $C_{16}H_{31}O_2^-$ (average 255.230 *m*/*z*) that is used to represent the remaining long-chain palmitic acid component of the binding medium. The third (*bottom*) row of images corresponds to the emission distribution of $C_{18}H_{35}O_2^-$ (average 283.262 *m*/*z*) that represents the remaining long-chain stearic acid component of the binding medium. The first column is the CdS reference showing (A) $CdC_2O_4^-$ emission distribution, MC = 3, TIC = 1.341×10^3; (B) $C_{16}H_{31}O_2^-$ emission distribution, MC = 64, TIC = 1.579×10^5; (C) $C_{18}H_{35}O_2^-$ emission distribution, MC = 54, TIC = 1.026×10^5. The second column is sample S6 showing (D) $CdC_2O_4^-$ emission distribution, MC = 8, TIC = 2.890×10^3; (E) $C_{16}H_{31}O_2^-$ emission distribution, MC = 7, TIC = 2.448×10^3; (F) $C_{18}H_{35}O_2^-$ emission distribution, MC = 3, TIC = 7.210×10^2. The third column is sample S112-2 showing (G) $CdC_2O_4^-$ emission distribution, MC = 5, TIC = 1.955×10^3; (H) $C_{16}H_{31}O_2^-$ emission distribution, MC = 68, TIC = 5.524×10^4; (I) $C_{18}H_{35}O_2^-$ emission distribution, MC = 16, TIC = 1.776×10^4. The fourth column is sample S115 showing (J) $CdC_2O_4^-$ emission distribution, MC = 9, TIC = 4.338×10^3; (K) $C_{16}H_{31}O_2^-$ emission distribution, MC = 12, TIC = 5.469×10^3; (L) $C_{18}H_{35}O_2^-$ emission distribution, MC = 31, TIC = 1.852×10^4. The fourth row is sample S117 showing (M) $CdC_2O_4^-$ emission distribution, MC = 4, TIC = 3.744×10^3; (N) $C_{16}H_{31}O_2^-$ emission distribution, MC = 7, TIC = 1.381×10^4; (O) $C_{18}H_{35}O_2^-$ emission distribution, MC = 3, TIC = 2.366×10^3

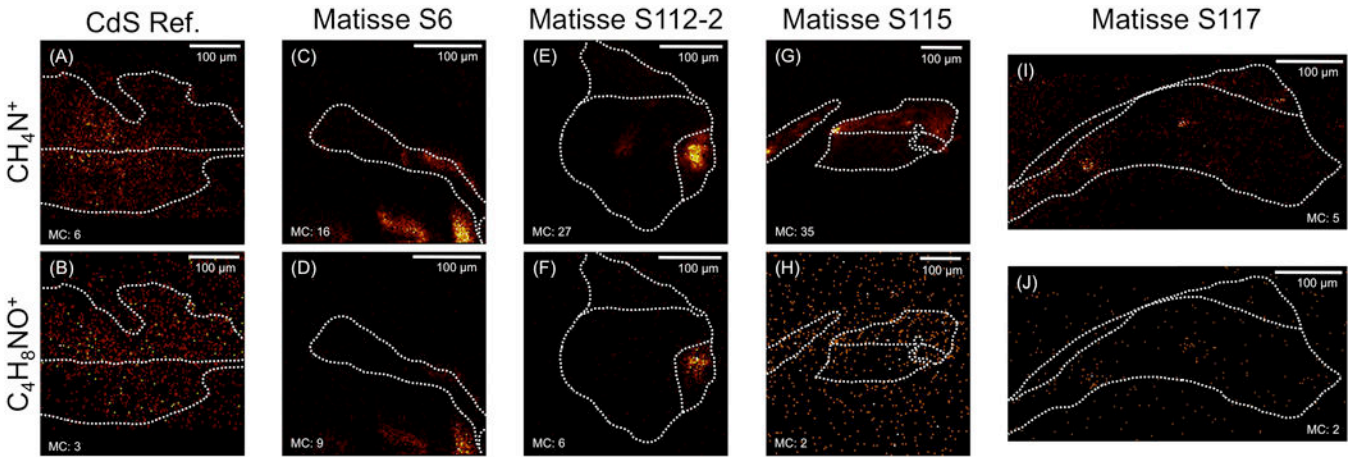

Fig. 6.

ToF-SIMS images of selected mass fragments associated with amino acid markers observed in the cross-sectional samples taken from *Le Bonheur de vivre. Dotted outlines* correlate to described layers in Fig. 1. The first (*top*) row of images corresponds to the emission distribution of CH_4N^+ mass fragment (average 30.033 *m*/*z*) that is used to represent the amino acid glycine (GLY), as well as generic amino acid fragment. The second (*bottom*) row of images corresponds to the emission distribution of $C_4H_8NO^+$ mass fragment (average 86.065 *m*/*z*) that is used to represent the amino acid hydroxyproline (HYP) that is used as a univariate identifier for the presence of collagen protein. The first column is the CdS reference showing (A) CH_4N^+ emission distribution, MC = 6, TIC = 3.306×10^3; (B) $C_4H_8NO^+$ emission distribution, MC = 3, TIC = 1.527×10^3. The second column is sample S6 showing (C) CH_4N^+ emission distribution, MC = 16, TIC = 6.415×10^3; (D) $C_4H_8NO^+$ emission distribution, MC = 9, TIC = 1.428×10^3. The third column is sample S112-2 showing (E) CH_4N^+ emission distribution, MC = 27, TIC = 6.429×10^3; (F) $C_4H_8NO^+$ emission distribution, MC = 6, TIC = 5.380×10^2. The fourth column is sample S115 showing (G) CH_4N^+ emission distribution, MC = 35, TIC = 1.084×10^4; (H) $C_4H_8NO^+$ emission distribution, MC = 2, TIC = 7.560×10^2. The fifth column is sample S117 showing (I) CH_4N^+ emission distribution, MC = 5, TIC = 2.057×10^3; (J) $C_4H_8NO^+$ emission distribution, MC = 2, TIC = 2.820×10^2

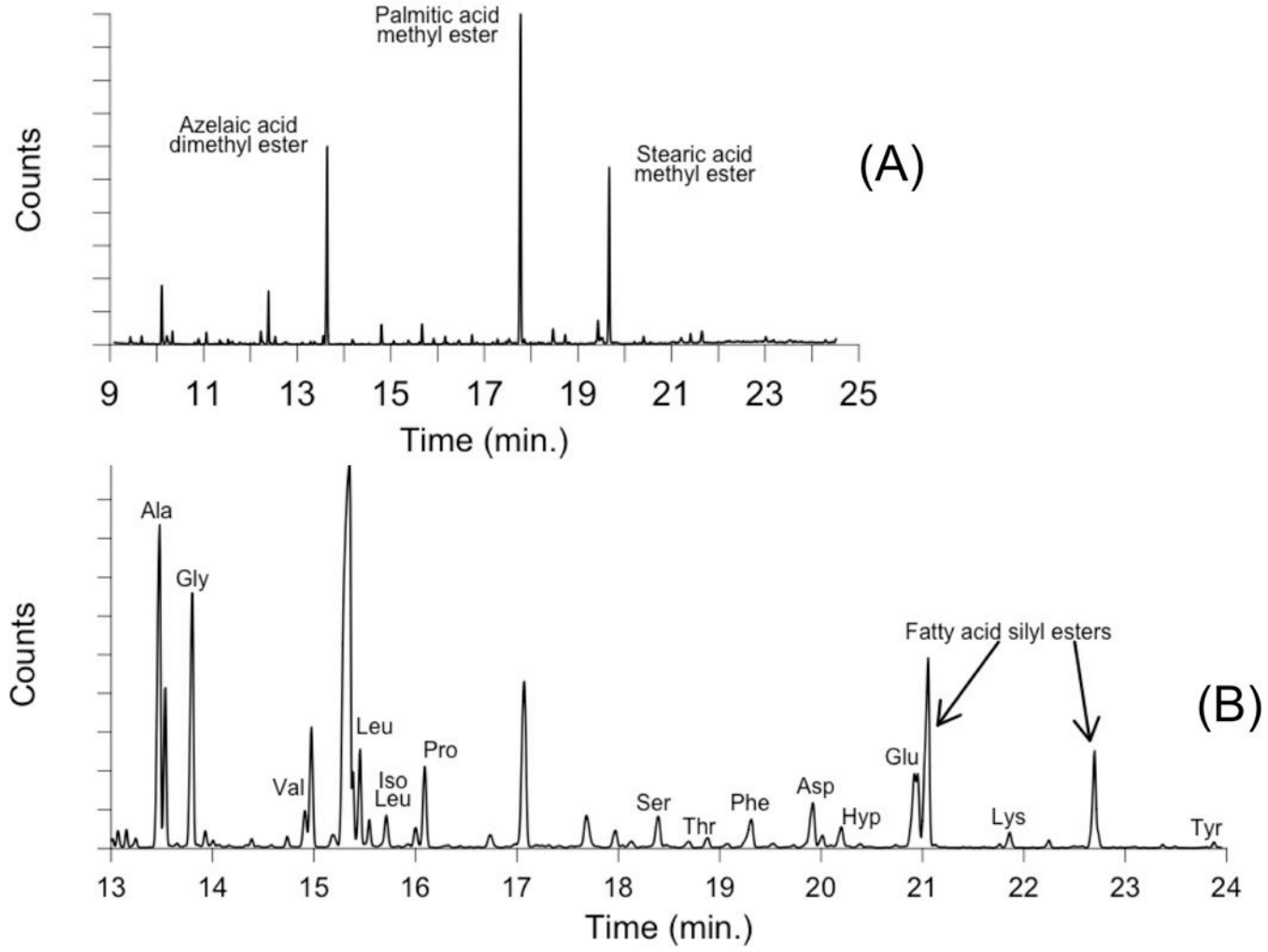

Fig. 7.

Results of the GC–MS analysis performed on two samples taken from the outer edge of *Le Bonheur de vivre* confirming the identification of long-chain fatty acids and amino acid fragments in the painting. Chromatogram (A) is from the fatty acid derivatization, and chromatogram (B) is from the amino acid derivatization as detailed in the text. Because the GC–MS analysis requires digestion of an entire sample, it is unclear the spatial positioning of the identified compounds in the chromatograms

Table 1

Comparison of expected isotope ratios versus calculated isotope ratios for the $CdCl^-$ mass fragment in the pure $CdCl_2$ reference powder and *Bonheur de vivre* sample S115, as shown in Fig. 2

Isotopic mass (*m*/*z*)	Expected isotope ratio (%)	Observed isotope ratio (%)	
		$CdCl_2$ standard	Matisse S115
140 875	0.95	1.09	0.99
142.872	0.98	1.03	1.11
144.872	9.68	9.97	7.37
145.873	9.70	9.67	9.65
146.870	21.31	21.20	18.51
147.872	12.36	12.12	9.98
148.873	27.62	27.38	26.78
149.870	2.96	3.21	5.57
150.871	12.63	12.46	14.24
152.871	1.81	1.87	5.60